Marine Structures 96 (2024) 103630

Contents lists available at ScienceDirect

Marine Structures

journal homepage: www.elsevier.com/locate/marstruc

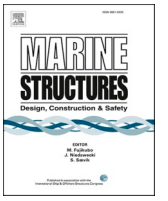

Assessing suction bucket jacket foundation installations in the South China Sea: Insights from field installation experiences

Lunbo Luo [a], Zhi Li [b], Zefeng Zhou [c,*], Weichen Wang [d], Wentao Wang [d]

[a] Science and Technology Research Institute, China Three Gorges Corporation, 2 Liangshi Road, Beijing, 101199, China
[b] Business Department of Renewable Energy, China Three Gorges Corporation, 1 Liuhe Road, Wuhan, 430010, China
[c] Advanced Modelling, Offshore Energy Norwegian Geotechnical Institute (NGI) Sognsvn. 72, 0855, Oslo, Norway
[d] Key Laboratory of Marine Environment and Ecology, Ministry of Education, Ocean University of China, 238 Songling Road, Qingdao, 266100, China

ARTICLE INFO

Keywords:
Suction bucket jacket
Installation
Layered soil
Penetration resistance
Parameter evaluation

ABSTRACT

The suction bucket jacket foundation has become a widely choice for supporting offshore wind turbines. Assessing the installation of the suction bucket foundation (SBF) is important as it significantly affects the stability of the offshore wind system and the overall project cost. Currently, experience with suction bucket jacket foundation installations primarily revolves around stiff clay and dense sand, drawing insights from North Sea projects (e.g. the design method reported by DNV-RP-C212). However, there is a shortage of publicly available knowledge concerning SBF installations in the South China Sea, characterised by deep-covered mud (i.e. very soft clay) and extensive layered soils. Existing design parameters may not adequately address these challenges, highlighting the need for a site-specific installation design method. This study introduces a tailored approach for evaluating design parameters of the SBF installation in the seabed conditions of the South China Sea. Utilising field data from 19 suction bucket jacket installations across the region, the proposed method undergoes rigorous validation and testing. The findings of this study aim to contribute to the advancement of offshore SBF installations in the intricate geological setting of the South China Sea. By presenting the SBF installation design method, the research offers practical guidance for both the evaluation of suction bucket jacket foundation installations and the optimisation of turbine locations in the region.

1. Introduction

Suction bucket foundation (SBF) is a competitive foundation type for offshore wind development [1–3]. Typically employed in jacket structures with three or four bucket foundations, the system is installed by evacuating water through the buckets using pumps, see Fig. 1. Recognised for its high installation efficiency and short construction period, the SBF has become a preferred choice in the industry. The SBF foundation's efficiency has been acknowledged since the 1980s when it began gradual and widespread use in the offshore oil and gas sector. Since 2014, it has found application in the offshore wind power field as well [4]. In China, SBFs have also begun to be applied and installed in several wind farms in recent years as highlighted in Table 1.

The installation of the suction bucket foundation (SBF) comprises two distinct phases: the self-weight penetration phase and the

* Corresponding author.
E-mail addresses: lunbo.luo@foxmail.com (L. Luo), li_zhi2@ctg.com.cn (Z. Li), Zefeng.zhou@ngi.no (Z. Zhou), wwc_0813@stu.ouc.edu.cn (W. Wang), wangwentao@stu.ouc.edu.cn (W. Wang).

https://doi.org/10.1016/j.marstruc.2024.103630
Received 2 December 2023; Received in revised form 20 March 2024; Accepted 1 April 2024
Available online 8 April 2024
0951-8339/© 2024 The Authors. Published by Elsevier Ltd. This is an open access article under the CC BY license (http://creativecommons.org/licenses/by/4.0/).

suction penetration phase. During the initial phase, as the SBF is gradually lowered to penetrate the seabed, its skirt autonomously penetrates to a specific depth. This process continues until the resistance encountered equals the SBF's self-weight [5–8]. Following this, the suction penetration phase commences. In this phase, the suction pressure is applied to enable further penetration until the target penetration depth (TPD) is reached [9–12]. Accurately assessing the magnitude of suction pressure is critical, as it must balance the penetration resistance against the SBF's self-weight. Proper assessment is crucial in preventing complications such as soil plug failure within the skirt [13] and mitigating the risk of skirt buckling [14]. This not only ensures the structural integrity of the installation but also significantly reduces both the costs and risks associated with offshore installations. Therefore, a precise evaluation of the SBF's penetration resistance is of paramount importance.

The calculation of the bucket foundation penetration resistance is recommended by two types of methods. One is the analytical method derived from both the conventional bearing capacity theory and the pile design method [15]. This approach involves undertaking numerous laboratory tests to ascertain critical geotechnical parameters, such as undrained shear strength, friction angle, relative density, and lateral earth pressure coefficient. However, these procedures can be somewhat laboratory-intensive and rely heavily on the quality of the geotechnical lab tests. Another one is the CPT-based empirical method recommended by DNV-RP-C212 (2021). In this method, only the measured cone penetration resistance (q_c), along with corresponding design parameters (that will be described later), is utilised to calculate the tip resistance of the SBF and friction resistance. This approach is relatively straightforward and widespread adopted [16–19]. However, it's essential to note that the design parameters recommended by DNV-RP-C212 (2021) are only suitable for North Sea conditions, where dense sand and stiff clay are prevalent in offshore wind farms (OWFs) [20–24]. However, the existing design method are not directly applicable to OWFs in China. This region experiences the transport of copious soft sediments discharged from the Yellow River and Yangtze River into the Yellow Sea, carried southward by the Jiangsu Coastal Current [25] to the South China Sea. The dynamic course changes of the Yellow River throughout the Holocene since 2278 BCE have led to the widespread distribution of very soft and layered soils nearshore [26], as illustrated in Table 1. Moreover, the design parameters for these sediments, characterised by very soft clay and intermediate soils (e.g., silt or silty mixtures), are notably absent in DNV-RP-C212 (2021).

The assessment of penetration resistance encounters complexities in the South China Sea owing to the unique soil characteristics. The distinct installation velocities during the self-weight penetration (SWP) and suction penetration phases can introduce varying

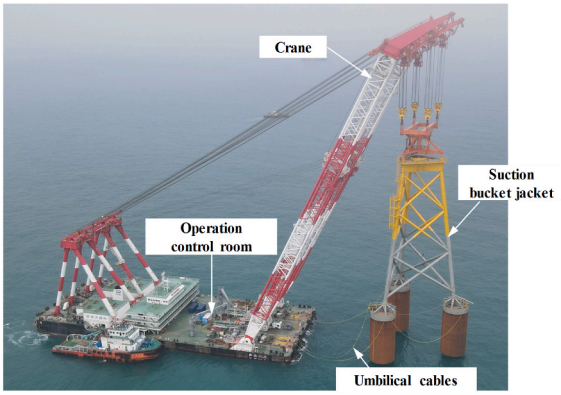

(a) installation system for a suction bucket jacket

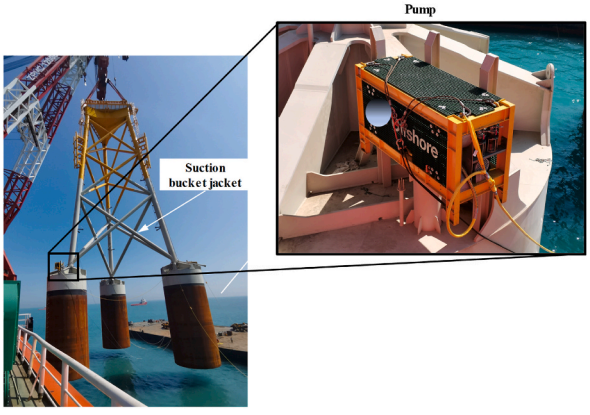

(b) Pump on the suction bucket

Fig. 1. Installation of a suction bucket jacket in South China Sea.

Table 1
Installed wind farms utilised SBF foundation in China [3,48,49].

Name	Number of applications	Water depth (m)	Type of foundation	Typical soil stratifications from seabed
Zhuanghe, phase I	3	15–20	Tripod bucket foundation	Soft clay, mud, sand and gravel
Zhuanghe, phase II	20		Tetrapod bucket foundation	
Shapa, phase I	3	28–30	Tripod bucket foundation	Clay, fine sand, medium-coarse sand, bedrock
Shapa, phase V	4	20–25		
Houhu	1	26		Soft clay, sandy silty clayey mixture, silty sand, silty clay, silty sand, silty clay, silty sand, coarse sand
This study	19	30–40		Mud, muddy soil, silty clay, silty sand

drainage conditions and seepage degrees, consequently impacting soil resistance. The SWP phase with a relatively rapid velocity induces an undrained condition in clay and silt, and a partially/fully drained condition in sand. Conversely, the suction penetration phase, with a comparatively slower velocity, results in an undrained condition in clay, a partially drained condition in silt, and a fully drained condition in sand. Field measurements indicate that the penetration velocity of the bucket foundation varies, ranging from approximately 1 to 5 m/min during the SWP phase and 1–5 m/h in the suction penetration phase. In this study, average velocities of 3 m/min for the SWP and 3 m/h for suction penetration have been selected for analysis. This decision is based on the observed range and aims to provide a representative understanding of the penetration process. The selection of these average velocities is critical for developing accurate design parameters that consider both soil type and drainage conditions, thereby ensuring a more precise assessment of penetration resistance in these complex geotechnical conditions. Relying exclusively on soil nomenclature (ignoring drainage condition) to establish design parameters for assessing penetration resistance could lead to a compromise in accuracy, especially in such complex scenarios.

This study aims to propose a new method applicable for evaluating the penetration resistance of SBF installations based on the CPT method. The classification of design parameters is based on the normalised velocity and drainage condition, diverging from the approach in DNV-RP-C212 (2021), which only considers clay and sand. This distinction is essential as it allows for the reflection of different mechanisms for one type of soil in two installation phases. 19 prototype SBF installations in the South China Sea are utilised,

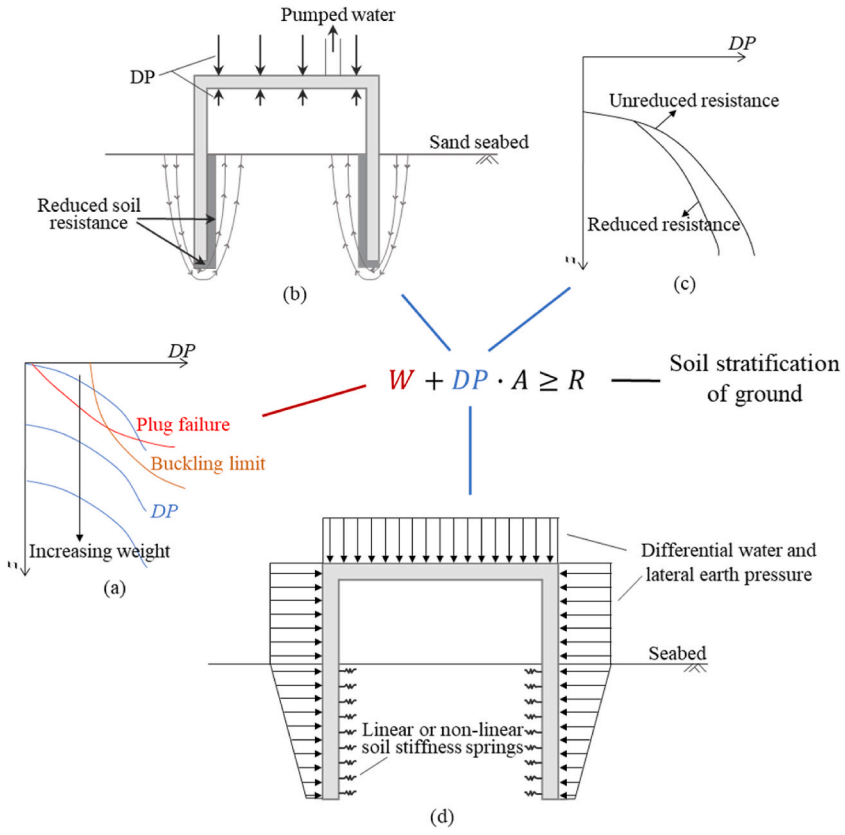

Fig. 2. Concept of the skirt penetration.

where 16 sites are analysed to propose a range of parameters suggestion and 3 sites are tested to verify the practicability. The insights gained from this analysis provide valuable guidance for designing SBF installations in the South China Sea, particularly considering the seabed conditions prevalent in the region. This methodology not only enhances the understanding of soil behaviour during SBF installation but also contributes to more efficient and effective design strategies for offshore wind energy infrastructure.

2. Method of calculation for suction bucket installation

2.1. Concept of skirt penetration

The installation of SBFs consists of two main phases: the self-weight penetration phase and the suction penetration phase. The process needs to be satisfied with the equation:

$$W + DP \geq R \tag{1}$$

where W is the buoyant gravity weight of the SBF, DP is differential pressure within the bucket induced by pumping water out of the bucket and R is the total geotechnical resistance, including the tip resistance R_{tip} and friction resistance R_{side} of bucket skirt. Eq (1) reflects that the force driving the SBF penetration must be equal to or greater than the total resistance R. The concept of Eq. (1) is schematically illustrated in Fig. 2.

Fixed wind turbine SBF foundations typically consist of three or four suction buckets underneath a jacket structure. These are set down on the seabed and installed together [27]. Therefore, in Eq. (1), the W term is the sum of the buoyant gravity weight of single bucket plus the jacket divided by the number of the buckets, assuming equal distribution of the jacket's mass among each bucket. The assumption is that SBF is sunk in a quasi-static state, essentially without the inertia force, ending the self-weight penetration phase at the depth where R equals W. Increasing W enables the SBF to reach a deeper depth in this phase. The benefits include facilitating closer proximity to the target penetration depth (TPD), reducing the required subsequent suction pressure and engineering risks. It also prevents unsealed spaces inside the bucket on uneven seabed, which could impact subsequent suction installation [28], and allows starting suction at a deeper location, beneficial for reducing buckling risks (Fig. 2(a)).

Following the self-weight penetration, pumping is applied to further drive the SBF towards the TPD [29]. The driving force is generated by the pressure difference between the inside and outside the SBF. In addition, seepage in pure sand seabed can reduce the tip resistance and friction resistance inside the skirt as shown in Fig. 2(b). Hence, the applied suction pressure can be lower than that for intact resistance (Fig. 2(c)). For thin-walled steel circular structures, high suction force may induce buckling failure (Fig. 2(d)). Consequently, there is a threshold value for applied DP (defined as buckling limit profile), which will be discussed later.

The total resistance R of SBF is linked to the soil stratification and ground properties, determinable through lab and in-situ tests. The penetration resistance during SBF installation is overcome by two parts: W and DP. The available or allowable DP is considered as a definite value once the geometry and the materials of SBF and soil properties are established. Accurate evaluation of resistance R is critical to estimate weather the sum of W and allowable DP can drive the SBF to reach the TPD.

2.2. Penetration resistance of SBF

There are two dominant methods for evaluating penetration resistance. The analytical method, based on bearing capacity theory [30], is expressed as:

$$R = R_{tip} + R_{side} = q_{tip}A_{tip} + f_s A_{side} \tag{2}$$

where q_{tip} is the end bearing capacity factor, A_{tip} is the end area of skirt, f_{s} is the unit friction factor, A_{side} is the area of skirt. Details are illustrated in DNVGL-RP-E303 [31].

This approach has a systematic theoretical background with respect to the shallow foundation and the conventional pile design, but it's application in practical engineering relies on a large number of lab tests to determine the soil parameters, i.e. soil unit weight, undrained shear strength of clay, the friction angle and the relative density of sand, and the lateral earth pressure coefficient. This can be cumbersome and less accurate in complex layered soils.

Alternatively, the empirical Cone Penetration Test (CPT) method [32] calculates penetration resistance using measured cone resistance q_{c} and empirical coefficients:

$$R = k_p(d)A_p q_c(d) + A_s \int_0^d k_f(z) q_c(z) dz \tag{3}$$

where k_p is empirical coefficient relating q_{c} to tip resistance, k_f is empirical coefficient relating q_{c} to friction resistance, d is the penetration depth, A_{s} is side area of skirted with per unit penetration depth.

The design parameters k_p and k_f are typically derived from field tests, which account for the effects of drainage in the seabed during the installation. Consequently, the CPT method can incorporate the reduction of penetration resistance in sandy conditions, an aspect not covered by the analytical method. Moreover, the CPT method offers simplicity and direct applicability for engineers in the design of SBF installations. Therefore, in this study, CPT method has been adopted and the design parameters is evaluated based on the field

tests in South Sea of China.

2.3. Limits to differential pressure

As outlined in Section 2.1, the applied DP must not exceed a certain threshold, herein referred to as the critical pressure. This ensures the integrity of both the skirt structure and the soil plug within the bucket. The primary concerns include soil plug failure, piping and the skirt buckling failure.

Soil plug failure: This encompasses soil plug uplift and reverse bearing failure [33]. In scenarios where undrained soil overlays drained soil, high suction force may cause plug uplift, a factor that must be carefully considered in practical design [34]. Reverse bearing failure may occur at pure clay conditions when the applied suction exceeds the reverse end bearing capacity of the soil, as detailed in Skempton [35].

Piping in Drained Soil: In soils like sand or coarser materials, upward seepage can occur, decreasing the resistance at the skirt tip. When the critical hydraulic gradient is achieved, 'ratholing' forms, potentially leading to piping as the effective stress is reduced to zero [36]. This would hinder the SBF from penetrating further to the TPD.

Buckling Failure of Thin Shell Structures: Under internal suction pressure, thin shell structures are prone to buckling [37]. During SBF installation, the surrounding soil could provide a support to overcome or avoid the occurrence of buckling to some extent, depending on factors like the soil type, soil strength and stiffness, and the effective supported length of skirt. Buckling failure adversely affects both further penetration and the in-place bearing capacity of the SBF. To simulate these conditions, finite element analysis using linear or non-linear soil springs can be employed by both geotechnical and structural engineers, as shown in Fig. 2(d). Besides, internal skirts or ring stiffeners by preemptive setup could enhance the buckling capacity of structure. Moreover, it is essential to note that the evaluation of suction bucket installation often involves two main constraints: structural buckling and cavitation pressure limits. While the buckling limit is linked to the bucket structure's design, the cavitation limit is predominantly determined by the water depth. This study focuses on the structural buckling limit of the SBF installation. In this particular context, the cavitation pressure limit generally exceeds the buckling limit, thereby justifying the exclusion of cavitation analysis from the study.

3. Evaluation of SBF installation in South Sea of China

This section will introduce a new strategy for evaluating the design parameters of SBF installation, drawing insights from prototype field installations in the South Sea of China. Firstly, the relevant data, including the ground conditions, the information of SBF, results of cone penetration tests, measured DP in the bucket, buckling limits and the soil failure limit, are demonstrated and utilised. Following this, a flowchart of the strategy is introduced in detail, outlining how the design parameters effectively function in the wind farm in the South China Sea. The results of this evaluation are elaborated in Section 4.

Table 2
The physical property soil from sampling borehole.

Site	Layer (m)	Soil type	Unit weight γ (kN/m^3)	Coefficient of permeability k (cm/s)	One-dimensional compression modulus E_s (MPa)
1	0–0.5	Mud	14.5	2.00E-07	0.5
	0.5–4	Mud	15.3	2.00E-07	1.8
	4–10.4	Mud	15.5	2.00E-07	2
	10.4–13.5	Muddy silty sand	18.5	2.00E-03	5
	13.5–23.4	Silty clay	18.4	5.00E-06	4
	23.4–25.2	Silty sand mixed mud	20.3	2.00E-03	7
2	0–1.2	Mud	14.5	2.00E-07	0.5
	1.2–8	Mud	15.7	2.00E-07	1.5
	8–9	Muddy silty sand	20	1.00E-03	7
	9–12.5	Silty clay	18.6	5.00E-06	4
	12.5–16.75	Silty clay	18.9	5.00E-06	4.2
3	0–0.9	Mud	14.5	2.00E-07	0.5
	0.9–6.5	Mud	15.8	2.00E-07	2.3
	6.5–9.3	Mud	15.6	2.00E-07	2.4
	9.3–10.7	Muddy soil mixed sand	16.2	9.00E-06	2.7
	10.7–16.8	Silty clay mixed sand	18.6	9.00E-06	4.7
	16.8–18.6	Silty clay	18.5	5.00E-06	4.7
4	0–0.4	Mud	15.5	2.00E-07	0.5
	0.4–8.8	Mud	16	2.00E-07	1.8
	8.8–9.9	Muddy soil mixed sand	18	3.00E-07	3
	9.9–14.7	Silty clay mixed sand	18.5	5.00E-06	4.2
	14.7–21.2	Silty clay	18.9	5.00E-06	4.2

3.1. Ground conditions

In this study, borehole (BH) sampling data is adopted for analysing the soil condition, and four typical sites are outlined in Table 2, focusing on depths relevant to the final penetration depth of the SBF. It can be visualised intuitively that deep-covered mud (i.e. very soft clay) is widely distributed on the seabed, of which thickness ranges from 6.9 m to 11.5 m. Fig. 3 exhibits the borehole data for Sites 2 and 3 at depths of 0–5 m, highlighting notably dilute soil samples that challenge solid formation. This seabed composition markedly differs from the stiff clay dominant in the North Sea (reported by Ref. [38]). This is one of the reasons that the recommended design parameters in DNV-RP-C212 (2021) are inappropriate to utilise in the South China Sea. Specifically, the friction resistance of skirt in such soft clay might be overestimated, leading to an underestimation of the self-weight penetration depth. Furthermore, DNV-RP-C212 (2021) primarily addresses clay and sand, whereas the seabed in this study presents multiple soil types and complex stratification, as shown in Table 2. The absence of parameters for silty soil and mixed soil compositions necessitates a simplified approach to stratification, which will be discussed later.

3.2. Bucket information

Table 3 summarises the geometry and self-weight of SBF across all 19 sites. The term 'mass' refers to the combined weight of three identical suction buckets and the jacket structure above. For analysis purposes, the mass of a single SBF is calculated by dividing the total 'mass' by three, under the assumption of equal mass distribution across the buckets. Additionally, the SBFs' buoyancy in water is considered, represented by a buoyant factor f_b

$$f_b = \frac{W}{G} = \frac{G - F}{G} = \frac{\rho_s V g - \rho_w V g}{\rho_s V g} = \frac{\rho_s - \rho_w}{\rho_s} \tag{4}$$

where G is the gravity in area, which is calculated by $G = mg$ (m is the mass of SBF). F is the buoyancy in water. W is the buoyant weight in water. V is the volume of SBF. ρ_s is the density of SBF. ρ_w is the density of water. Hence, the buoyant factor is taken as 0.87 in this study, and the buoyant weight of SBF W is calculated by $W = f_b G$.

The installation pumping and data acquisition system used for SBFs, as depicted in Fig. 1(b), includes several key components. Each bucket is equipped with a pump at its lid, which plays a key role during installation. In the initial Self-Weight Penetration (SWP) phase,

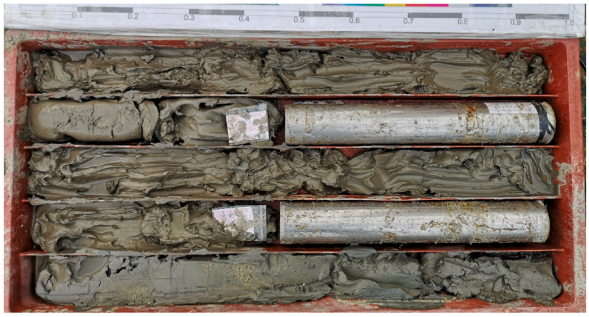

(a) site 2

(b) site 3

Fig. 3. Object of sampling borehole.

Table 3
The SBF information for 19 sites.

Site	Skirt height (m)	Outer diameter (m)	Skirt thickness (m)	Mass (kg)
1	26	10	0.035	2003680
2	17	15	0.032	1972340
3	19	13.5	0.032	2145440
4	21.5	10	0.035	1905390
5	21.5	10	0.035	1911430
6	19.5	10	0.045	1921400
7	21.45	12	0.035	2303575
8	21.45	12	0.035	2306875
9	19.5	10	0.045	1924200
10	19.5	10	0.045	1939900
11	22.5	12	0.045	2470156
12	21.5	10	0.03	1919540
13	21.5	11	0.048	2144410
14	21.5	10	0.03	1934960
15	19	13.5	0.032	2154930
16	22	13.5	0.032	2269930
17	19.5	10	0.045	1923900
18	22	13.5	0.032	2245950
19	22.5	12	0.045	2461156

the pumping valve remains open, allowing water to freely exit the bucket without inducing suction pressure. After completing the SWP, the pump activates to extract water, creating suction inside the bucket. This process is closely monitored; the flow rate is measured by a flowmeter, and DP is calculated using two total pressure sensors—one inside the bucket and another outside. The penetration depth of the bucket is accurately tracked via GPS and verified with an underwater Remotely Operated Vehicle (ROV). All pertinent data, including flow rates, pressure readings, and penetration depths, are continuously recorded and transmitted to the operation control system through an umbilical cable. This system has been effectively utilised in numerous suction bucket installations globally, proving its efficiency and reliability.

3.3. A new strategy for evaluation of kp and kf design parameters for SBF installation

The flowchart of the strategy is conceptually divided into two main aspects: 1) classifying soil stratifications, and 2) evaluating the design parameters, k_p and k_f, for each soil types in different penetration phases. The specific processes are schematically illustrated in Fig. 4, and explained in detail as follows.

Step 1. - ***soil classification***: In traditional static loading problems, such as bearing capacity failure of a shallow foundation, soil is typically classified by its nomenclature (i.e., clay, silt, or sand). However, during the installation of SBFs, the natural material may exhibit varying behaviors in response to different loading rates and drainage conditions [39]. To account for these variations, in this study, multiple soil types are classified into three categories: undrained soil (UDS), partially drained soil (PDS), and drained soil (DS).

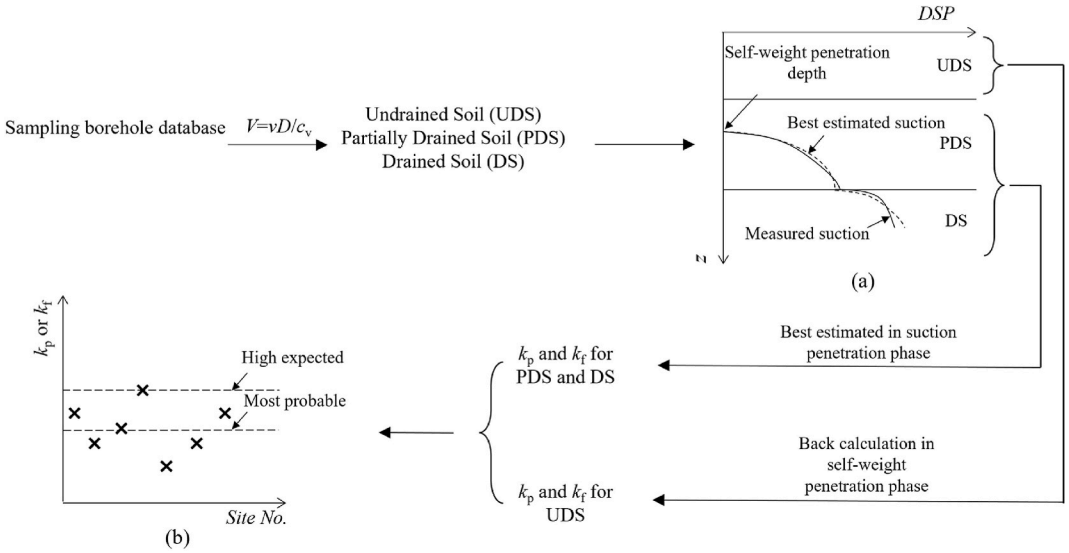

Fig. 4. Flowchart of the new strategy for evaluating the design parameters of SBF installation.

This classification is based on the normalised velocity V [40]:

$$V = vt/c_v \tag{5}$$

where v is the velocity of the SBF penetration, (based on field measurements, the average velocities are selected: v is about 3 m/min for self-weight penetration phase, and 3 m/h for suction penetration phase). t is the drainage path referred as the thickness of the skirted. c_v is the coefficient of consolidation and calculated as

$$c_v = kE_s/\gamma_w \tag{6}$$

here k is permeability of soil, E_s is the one-dimensional compression modulus and γ_w is the unit weight of water. The parameters for calculating V can be obtained from Tables 2 and 3.

Soils are classified based on V values: $V < 0.01$ indicates a drained soil condition, $V > 30$ indicates an undrained soil condition, and values between 0.01 and 30 indicate various degrees of partial drainage soil condition [41,42]. Hence, in this study, the soil in drained condition is referred to as DS, in undrained condition as UDS, and in partial drainage condition as PDS.

It is important to clarify that the nomenclature used in this study for classifying soils does not pertain to the intrinsic, characteristic properties of the soil. Instead, these classifications are context-specific, referring to the types of materials through which the SBF penetrates under particular conditions. This means that the classification results are only suitable for the SBF installation where the parameters of penetration velocity v and the drainage path t have been defined. Furthermore, it's essential to understand that this classification may not directly translate to other types of foundation installations. In scenarios where the dynamics of penetration velocity and drainage path differ, the same soil may be characterised differently, reflecting its behaviour under varying installation conditions.

Step 2. – ***self-weight penetration phase***: During self-weight penetration phase, the skirt tip of the SBF initially penetrates through the mud layer and stops at a layer with relatively high strength, like silt or silty clay. In these types of ground, the normalised velocity V of the SBF generally exceeds 30, whether in mud or silt, indicating an undrained condition. Consequently, an agreement is achieved that all the types of soil within the self-weight depth are considered as UDS. By the end of this phase, a force equilibrium of, W=R, is achieved. The resistance R in Eq. (3) can be calculated by Eq. (4), and the self-weight penetration depth d_s in the right side of Eq. (3) can be determined from the SBF installation data. Furthermore, In the context of the self-weight penetration phase, the cone penetration resistance q_c encountered in the softer soil is relatively low. Consequently, the parameter k_p and the associated tip resistance play a minimal role in contributing to the total resistance experienced during SBF penetration in such soils. To account for this, k_p for the UDS is set to a constant value. This value is aligned with the one recommended for clay in DNV-RP-C212 (2021). This allows for the back-calculation of the variable k_f for UDS in Eq. (3). This approach ensures that the evaluation of soil resistance during SBF installation is both accurate and consistent with established guidelines, particularly in conditions where the soil exhibits characteristics similar to undrained clay.

Step 3. – ***suction penetration phase***: During suction penetration phase, the rate of penetration is influenced by the DP induced by pumping flow. This results in a relatively slower penetration velocity, leading to conditions of partially drained soil (PDS) or drained soil (DS). To accurately estimate the parameters k_p and k_f, for both PDS and DS, a reliability-based method is adopted with measured DP considered. It can repeatedly iterate these two parameters to match the penetration resistance (subtracting W) with the measured differential pressure, until the relatively smallest error is achieved. The exact value of this error can not be defined or limited here, because either the q_c or the DP may exist uncertainty, which will be introduced in the following section.

In the evaluation process for SBF installations, accurately determining the parameters, k_p and k_f, within the same equation presents a complex challenge, akin to solving equations with indeterminate solutions. To address this, two distinct approaches are necessary: 1) For PDS, the q_c is similar to that in the UDS, leading to the setting of k_p for PDS equal to that of UDS, as well as the standard value for clay according to DNV-RP-C212(2021). Hence only k_f for PDS is used to best estimated. 2) A noticeable shift occurs when transitioning from PDS to DS, marked by a spike in both q_c and DP. In this scenario, the initial method is insufficient as k_p plays a pivotal role due to the increased tip resistance in DS. The adjustment only for k_f in DS couldn't capture this spike which is due to the larger tip resistance encountered. The strategy, therefore, involves initially keeping k_f constant while adjusting k_p to reflect the spike in the DP curve, as shown in Fig. 4(a). Subsequently, with a fixed k_p, the focus shifts to fine-tuning k_f to align with the measured DP, ensuring accurate parameter estimation under varying soil conditions during installation.

Step 4. In Step 4 of the SBF installation evaluation process, the determination of the parameters k_p for UDS and PDS was not explicitly outlined in Steps 2 and Step 3. Therefore, to address this, the back-calculated and best-estimated parameters across all sites are analysed to derive the most probable (average) and high expected (upper limit) values for k_p of DS and k_f of UDS, PDS and DS as shown in Fig. 4(b).

Additionally, a unique scenario is considered when the SBF encounters a sand layer during the self-weight penetration phase, potentially categorising the soil as PDS. In such cases, the back-calculation process for UDS outlined in Step 2 is disrupted. To address this, an alternative approach is employed: Step 3 is conducted first to determine the parameters for PDS during the suction penetration phase. Following this, these parameters are applied to Step 2, where the suction phase parameters for PDS are used to recalibrate the self-weight penetration phase. Subsequently, k_f for UDS is back-calculated. Notably, this revised approach was specifically implemented at two sites where this sand layer condition was encountered. At one site, the approach was used for back-calculated analysis,

while the other served as a practical test case to validate the methodology.

4. Results and discussion

In this section, the application of the newly developed strategy for SBF installations is examined across various sites. The methodology is first illustrated through case studies of three representative sites, showcasing the simplified soil classification process and the evaluation of parameters. This is followed by an analysis of the best-estimated parameters for the initial 16 sites, leading to a set of parameter recommendations. The final segment of the section employs the last three sites to test the applicability of these recommended values and to evaluate the feasibility of the proposed strategy. This comprehensive approach validates the strategy and assesses its practicality in diverse site conditions, offering a detailed insight into the efficacy of the methods used in the study. Due to confidentiality constraints and the uniformity of ground conditions among the three buckets at each jacket location, this study presents only one set of in-situ investigation data and DP measurements for a single bucket. The decision to limit the data presentation arises from the need to adhere to confidentiality agreements and the recognition that the ground conditions for the buckets within each jacket site are remarkably similar.

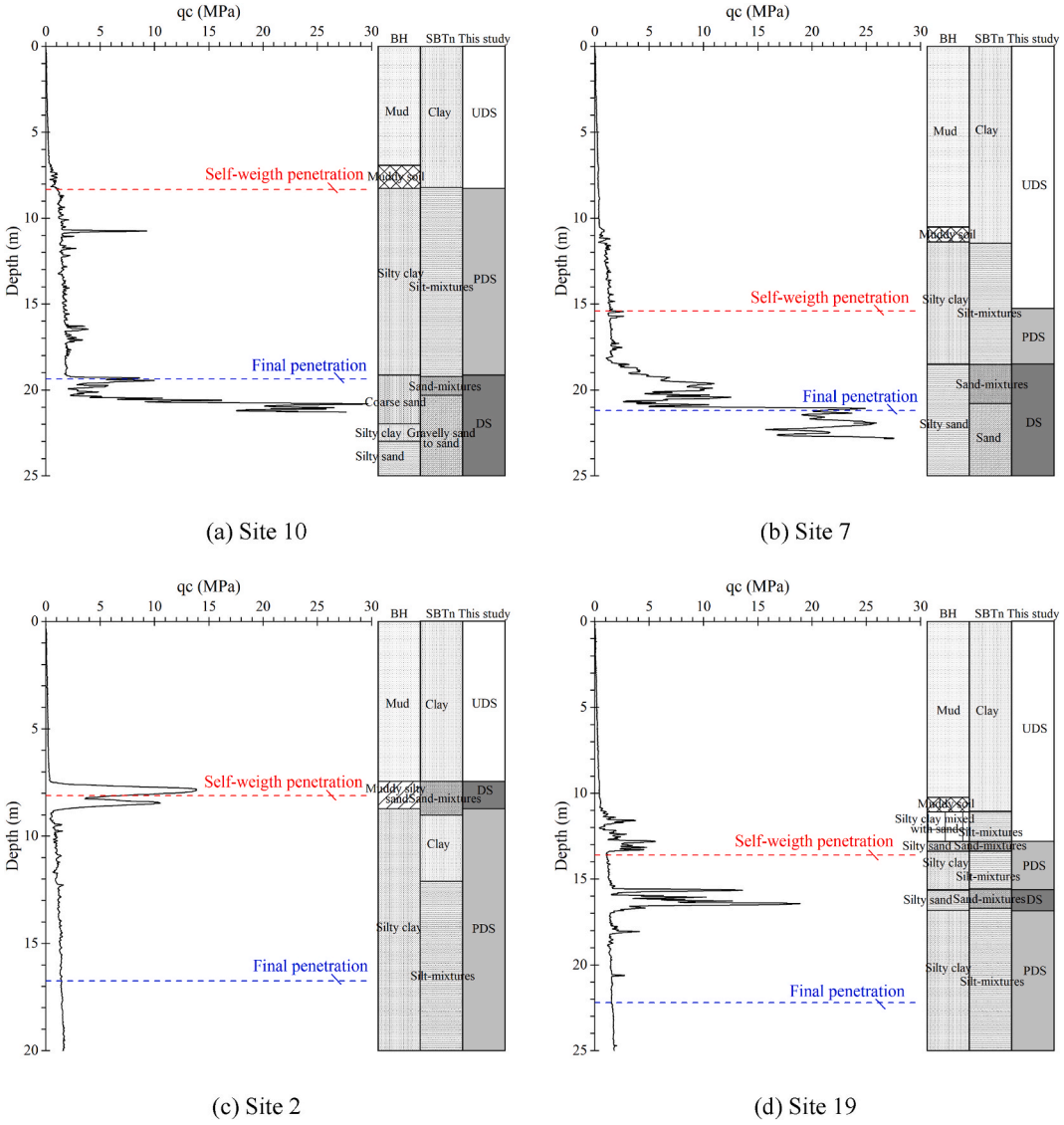

Fig. 5. Cone penetration resistance of four representative sites.

4.1. Soil classification and behaviour

Cone penetration resistance (q_c), measured by Cone Penetration Test (CPT), is a crucial parameter for evaluating Suction Bucket Foundation (SBF) installations, as illustrated at four representative sites in Fig. 5. With the measured q_c and borehole (BH) samplings, this study employs various soil classification methods to accurately understand soil behaviour specific to SBF installation. These methods include laboratory tests from BH samples, normalised soil behaviour type classification by CPT (SBTn) according to Robertson [43], and the normalised velocity approach. Observations reveal that q_c in clay up to 7 m below the mudline remains consistently low, not surpassing 1 MPa. This indicates that the resistance offered by the mud layer is minimal, typically allowing the SBF to penetrate without obstruction. In contrast, the maximum q_c value observed in sand does not exceed 30 MPa, which is significantly different from European conditions where q_c in sand has been reported to reach 60 MPa at a depth of just 2 m below the mudline, as noted by Bye et al. [21].

Site 10 represents a category of concise stratifications, as depicted in Fig. 5(a), where UDS is layered over PDS. This site configuration is particularly suitable for back-calculating the k_f of UDS and evaluating the k_f of PDS. Notably, a spike of q_c located at a very narrow range within 10.8–10.9 m is observed, possibly due to the skirt tip contacting a small stone. *Site 7* represents the category of stratification where the PDS is overlaid under the UDS layer and overlying the DS layer as shown in Fig. 5(b). This site is ideal for evaluating both k_p and k_f of DS using the method outlined in Section 3.3. Between depths of 11.35 and 18.7 m, a silty clay layer (identified by BH) is categorised into two distinct soil types for different installation phases. Consequently, the same soil type is assigned two different sets of design parameters based on the conditions encountered. Site 2 and 19 exhibits that a silty sand or sand layer is lied within the self-weight penetration phase. This soil layer, which is classified as DS in suction penetration phase, is classified into PDS in self-weight penetration phase as shown in Fig. 5(c and d). This distinction underscores the necessity of classifying soils in relation to different installation phases and corresponding design parameters, highlighting the dynamic nature of soil behaviour under varying installation conditions.

The classification by SBT chart [43] are exhibited in Fig. 6, whilst the soil behaviour type index, I_c, is shown in Fig. 7. These figures illustrate that soft clay, silt, and sand are predominant in the studied area, with the silt exhibiting more clay-like properties as indicated

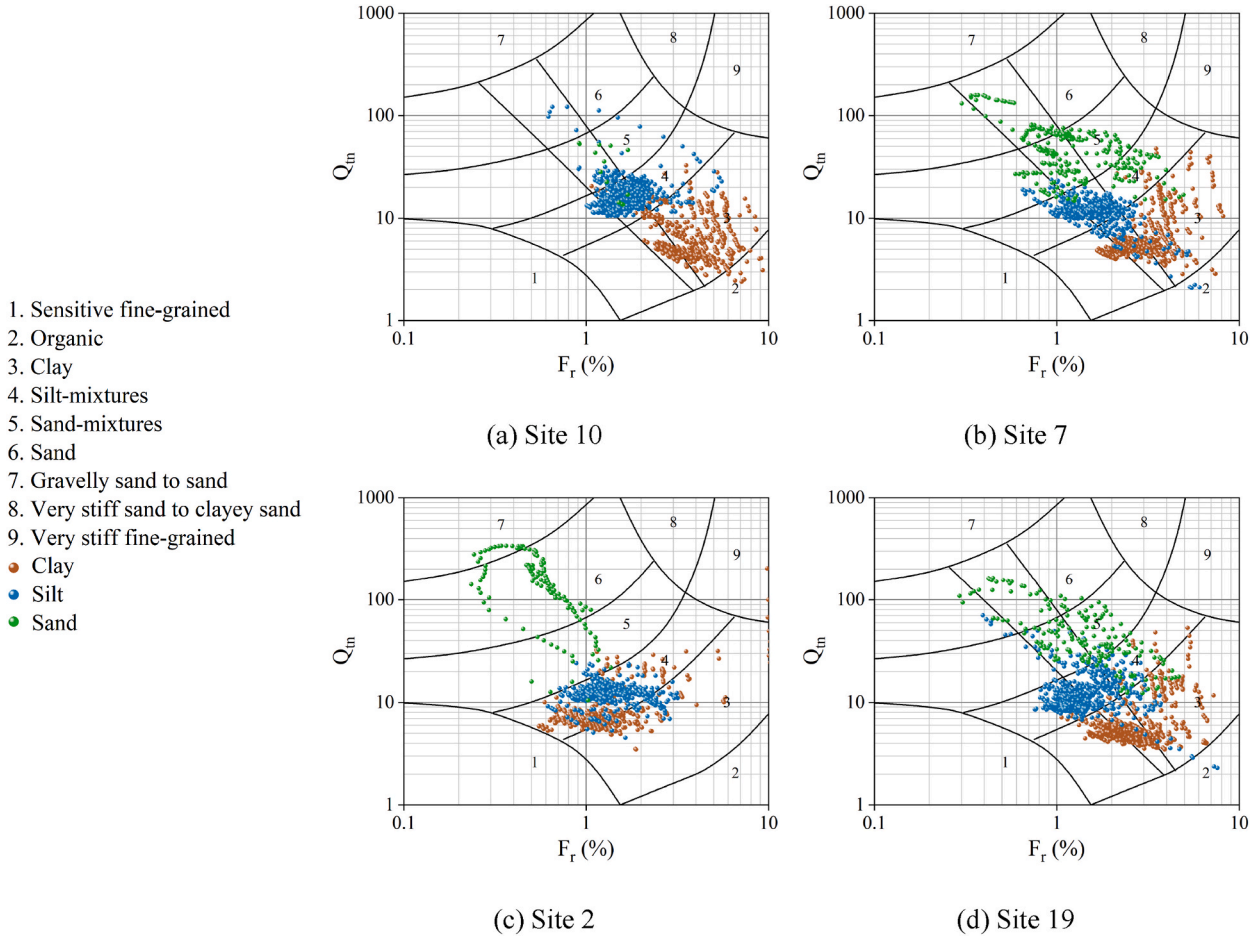

Fig. 6. Soil classification based on the SBTn chart of four representative sites.

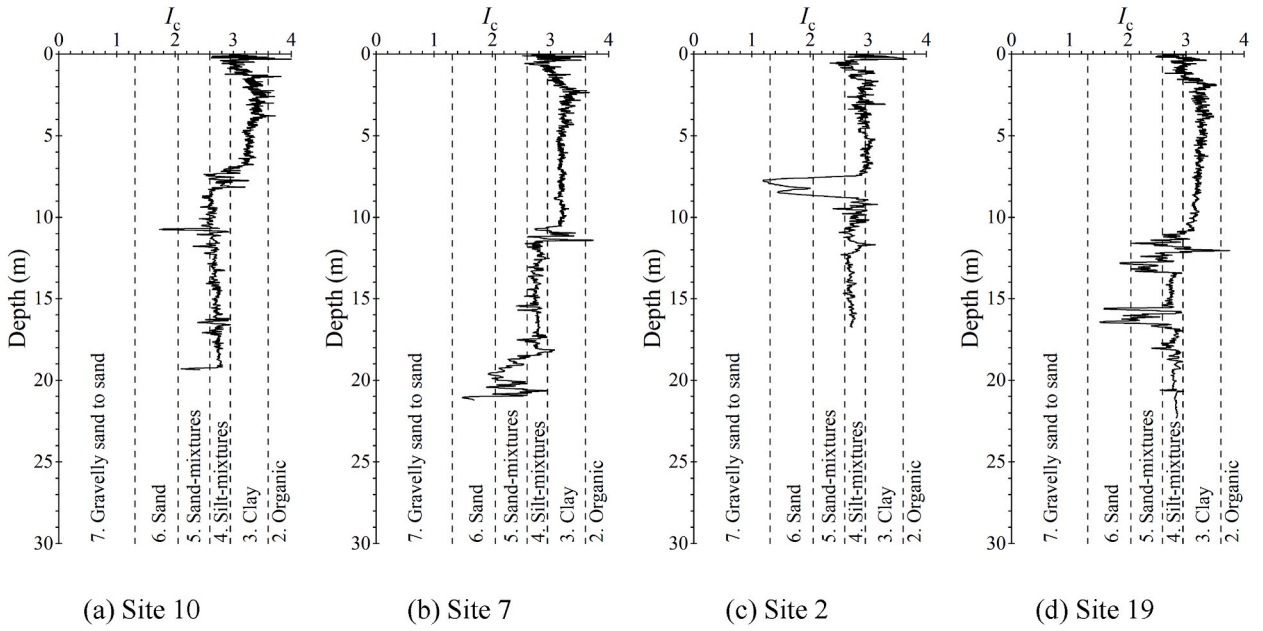

Fig. 7. The soil behaviour type index, I_c.

by an I_c value exceeding 2.6.

The results of the soil classification based on the normalised velocity for all 19 sites are shown in Fig. 8, where the numeric labels on each data point correspond to layer depth. A notable observation is that the normalised velocities for PDS tend to cluster within the range of 0.69–1.53. This range is numerically closer to the UDS boundary than to the DS, suggesting that the physical properties of PDS are more akin to undrained conditions. This characteristic will be leveraged in subsequent sections of the study. Additionally, the corresponding soil stratifications, as classified by borehole sampling, are listed alongside for comparison. It is observed that the same soil type, such as silty clay, is categorised differently under various installation phases and penetration velocities, being divided into UDS and PDS. This observation lends credence to the approach of classifying soil based on the specific installation phase and drainage conditions, affirming the rationale behind this method of soil classification for SBF installations.

4.2. Analysis for the design parameters

The results of the best estimated suction and measured DP are plotted in Fig. 9, in which the tendency and the comparability is observed. Measured DP could have some inaccuracy influenced by various factors such as interruptions in suction recording,

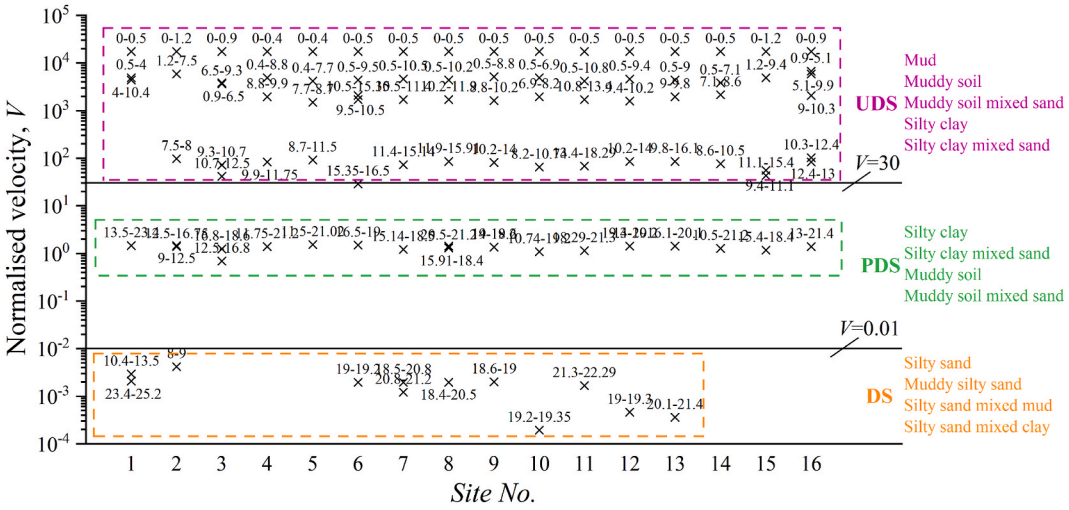

Fig. 8. Normalised velocity of all 16 sites.

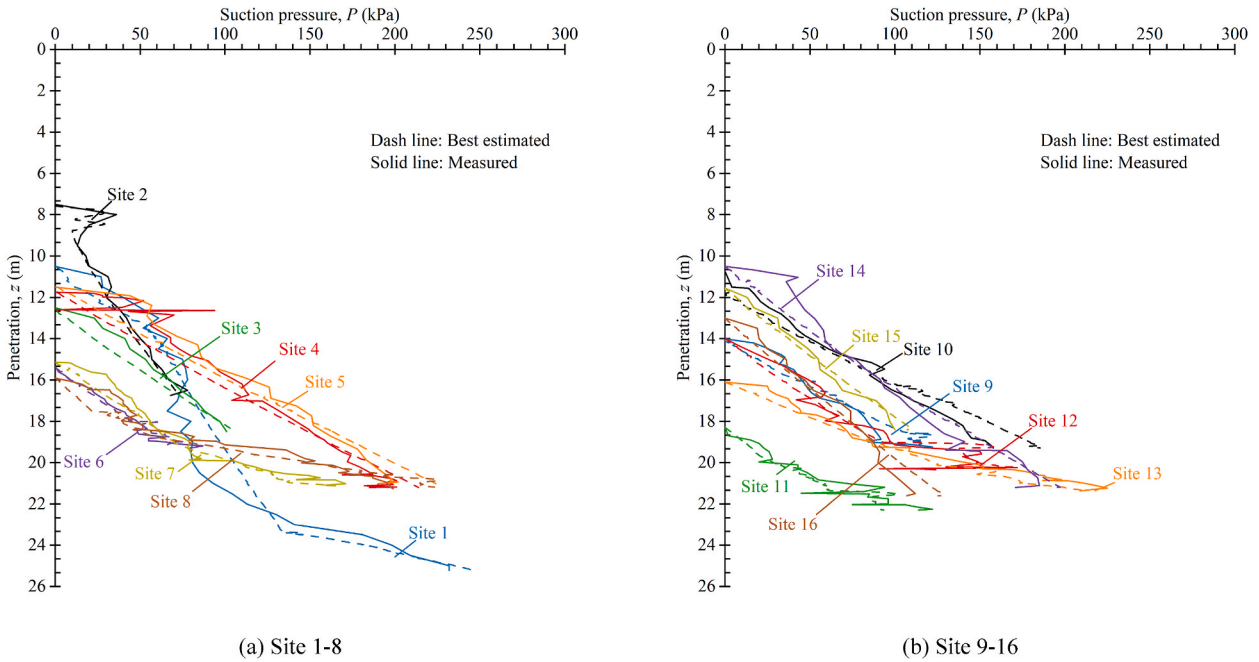

Fig. 9. Results of best estimated for the first 16 sites.

discontinuities in pumping, encounters with embedded stones, etc. Consequently, achieving highly accurate resistance estimation is challenging, with considerable error likely between the measured DP and the best estimations.

Fig. 10 displays the results of k_p and k_f from both back calculation and the best estimated evaluations across multiple sites. In some instances, two parameter values for a single soil type are noted, such as k_f for DS at site 1, due to an interlayer dividing the soil into distinct sections with different design parameters. Besides, the lack of parameters for DS at site 3–5 and 14–16 is due to the absence of DS layer existing.

Suggestion values for coefficients k_p and k_f for UDS, PDS and DS are listed in Table 4, where the most probable value is derived as an average from all sites, and the high expected value as the maximum. Summarization of k_p and k_f for model tests and prototype cases reported from the available publication are plotted in Fig. 11. The UDS, PDS and DS defined in this study are represented in terms of clay, silt, and sand merely as a form of presentation. It is important to note that the parameter range indicates minimum and maximum values, contrasting with DNV-RP-C212 (2021), which only proposes the most probable value without a minimum. Despite most cases being applied in sandy grounds, there is a significant discrepancy among them, suggesting the difficulty in identifying a single set of k_p and k_f values that would be universally applicable for evaluating SBF penetration resistances across all wind farms.

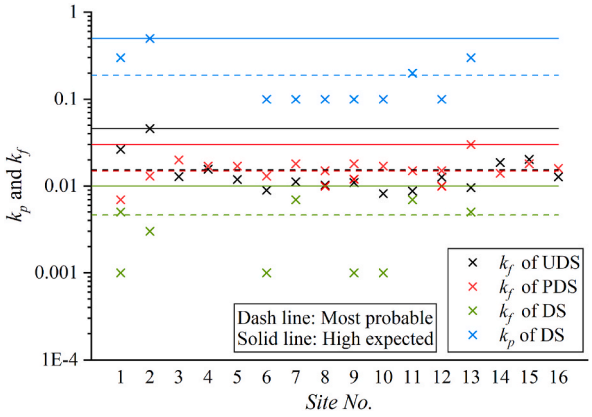

Fig. 10. Results of the back calculated and the best estimated and for k_p and k_f.

Table 4
Suggestion values for coefficients k_p and k_f for clay, silt and sand, South Sea of China.

Type of soil	Most probable (R_{prob})		High expected (R_{max})	
	k_p	k_f	k_p	k_f
UDS	0.4	0.0153	0.6	0.0457
PDS	0.4	0.0149	0.6	0.02
DS	0.19	0.0046	0.5	0.01

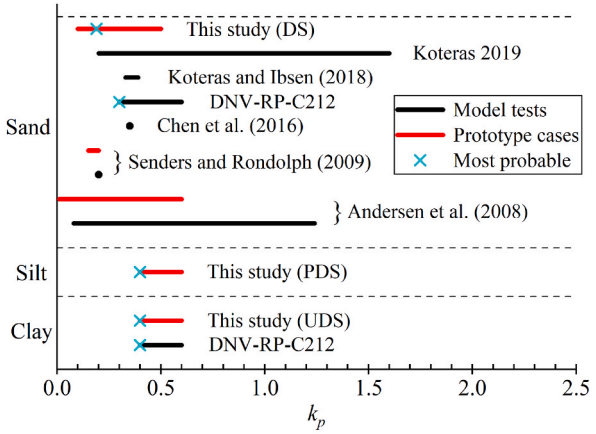

(a) kp

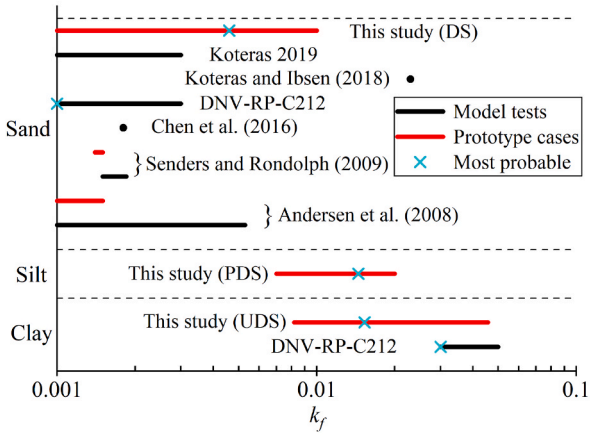

(b) kf

Fig. 11. Summarization of the kp and kf from the available publication and this study.

4.3. Case study for testing the suggested design parameters

This section presents a case study aimed at evaluating the effectiveness of the suggested design parameters for SBF installations. The case study focuses on applying the proposed parameters to three sites, providing insights into their practical utility and accuracy. The application procedure for design parameters is outlined as follows:

1. **Soil Classification for Self-Weight Penetration Phase:** Classify the soil within a sufficient depth based on criteria for the self-weight penetration phase (v = 3 m/min). In this phase, mud, clay, and silt are generally classified as UDS, while silt sand or sand are likely categorised as PDS, but as DS in the suction penetration phase.
2. **Calculation of Penetration Resistance:** Calculate the penetration resistance with corresponding parameters for the whole depth and confirm the self-weight penetration depth d_s where the resistance is equal to the buoyancy of the SBF W.

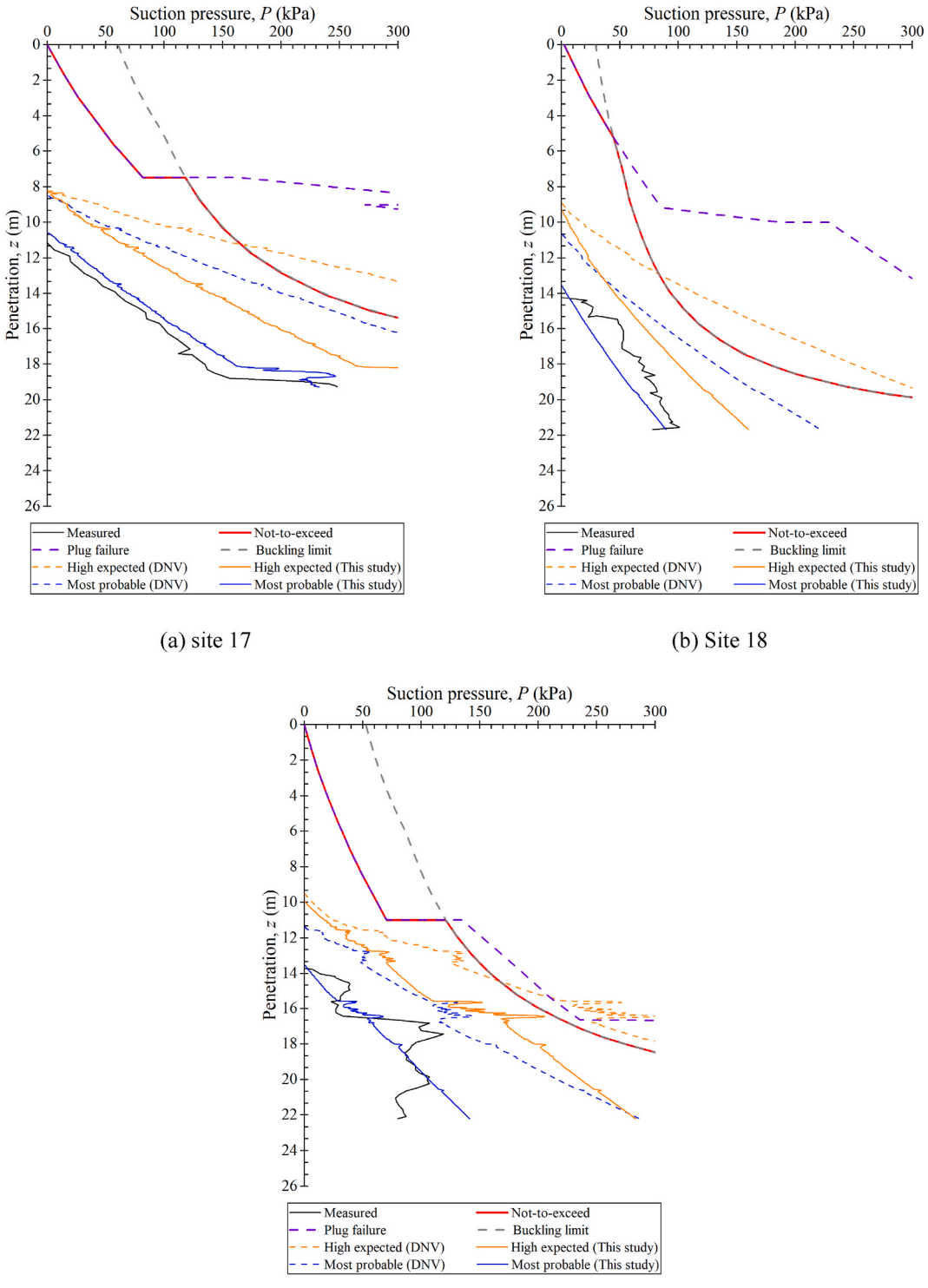

Fig. 12. Results of testing the suitable of the design parameters.

3. **Reclassification for Suction Penetration Phase:** Reclassify the soil for the depth d_s based on the criterion for the suction penetration phase ($v = 3$ m/h).
4. **Recalculation of Resistance:** Recalculate the penetration resistance beneath the depth d_s using the reclassified parameters from the previous step. Plot the DP curve by subtracting W, as well as the resistance at d_s, from the penetration resistance.

The results of application on 17–19 sites to test the applicability of the design parameters proposed above are plotted in Fig. 12. The matched q_c curves by CPT within the depth of TPD are plotted in Fig. 13. The predictions for self-weight penetration depth d_s are relatively accurate, with deviations of 0.67 m, 0.58 m, and 0.16 m for sites 17–19, respectively. The predicted most probable results for DP closely align with the measured DP, while the high expected results are more conservative.

The predicted results for Site 17 align closely with the actual measurements. A significant spike in resistance at a depth of 18.3–19.2 m, where the SBF tip encounters the DS layer, leading to high tip resistance, is accurately captured by the prediction. For Site 18, the predicted results exhibit a smooth trend, mirroring the q_c trend as depicted in Fig. 13. This consistency suggests that the soil at Site 18 is evenly distributed. However, the measured DP at this site shows fluctuations, which may be attributed to spatial differences between the CPT and SBF locations. In contrast, the predictions for Site 19 do not correspond as closely with the actual measurements. The predicted spike in q_c occurs at a depth of 15.56–16.86 m, whereas the spike in the measured DP is noted at a depth of 16.44–18.31 m. This discrepancy could be due to the inclined distribution of the soil layer at this site, indicating a variation in soil properties or layering that was not fully captured by the predictive model. This case underlines the complexity of accurately predicting soil behavior and SBF installation outcomes, especially in environments with varied or non-uniform soil stratifications.

The study also includes a comparison of results with the parameters outlined in DNV-RP-C212 (2021), applying the parameters specified for clay and sand to UDS and DS, respectively. Due to the lack of specific parameter suggestions for silt in DNV-RP-C212 (2021), the UDS parameters are used as a substitute for both silt and PDS. This additional information is deemed reasonable given that the normalised velocity of PDS in this particular wind farm is closer to UDS, as illustrated in Fig. 8. A key observation from the comparison is that the predictions based on DNV-RP-C212 (2021) parameters tend to be significantly higher than both the measurements and the predictions made in this study. This discrepancy is attributed to the larger parameter values listed in DNV-RP-C212 (2021) as shown in Fig. 11. Additionally, the range of the most probable and high expected results in this study is broader than that in DNV-RP-C212 (2021). This wider range can be explained by the diverse coverage of soil types encountered in the studied ground, leading to a broader spectrum of parameter values. This analysis highlights the importance of considering site-specific soil characteristics and suggests that a more nuanced approach, as proposed in this study, may provide more accurate predictions for SBF installations in varied soil environments. Additionally, from a practical perspective, the design parameters and the four-step installation assessment method are proven to be effective for the South China Sea, their application to other locations requires careful consideration of local geotechnical conditions. The current scarcity of sufficient and comparable installation data in other regions limits the universal application of the findings. Nonetheless, as more data becomes accessible in the future, there will be ample opportunities to further test and validate our approach in a variety of geotechnical settings, enhancing its applicability and relevance across different offshore environments.

4.4. Discussion

Several factors contribute to the challenges in predicting penetration resistance with high precision in SBF installations. Firstly, in these 16 sites, the values of normalised velocity V are located in a limited range of 0.65–1.53 for PDS, but in a wide range of 41.37–17500 for UDS and 0.000194–0.00414 for DS as shown in Fig. 8. This variation indicates that a single set of parameters for UDS or DS may not be sufficient to encompass the diversity of soil types encountered. Therefore, a more detailed classification of soils, coupled with multiple sets of parameters, could potentially enhance the accuracy of penetration resistance predictions. The quality of CPT data is another critical factor, as evidenced by sites 18 and 19. Accurate CPT data that faithfully represents soil stratification is crucial for evaluating penetration resistance precisely. A recommendation is made to conduct multiple CPTs (2 or 3) around each bucket (for the challenging site), if feasible, to better ascertain the distribution of soil layers around and beneath the SBF. Furthermore, the seepage effect in pure sand sites significantly influences design parameters. During the suction penetration process, seepage inside the skirt is likely to generate an upward force, which reduces the effective stress of soil, thereby affecting the penetration resistance, especially the tip resistance in sand. In the case of the wind farm site studied, the presence of a thick clay layer above the sand layer serves to mitigate this seepage effect. Although the seepage effect was not a primary consideration in the development of the design parameters due to this specific geological context, the four-step strategy outlined in the study remains applicable in seabeds where seepage is a significant factor. This strategy can be adapted to account for the seepage effect, ensuring accurate prediction of penetration resistance in diverse seabed conditions. Additionally, the process of SBF landing on the seabed is typically assumed to occur at a sufficiently low velocity, mimicking a quasi-static state without significant dynamic response. However, in reality, the inertia force of the SBF might slightly deepen the self-weight penetration depth, potentially leading to an underestimation of soil resistance. Lastly, the limited data from the 16 sites do not provide a comprehensive basis for suggesting universally applicable design parameters. Therefore, further studies incorporating more SBF installation cases are anticipated to refine and update the design parameters proposed in this study, thereby improving the reliability and applicability of the predictive models.

5. Mitigation measurements

The penetration resistance of SBF installation introduced above in section 2.2 and 2.3 are only suitable for the idealised conditions.

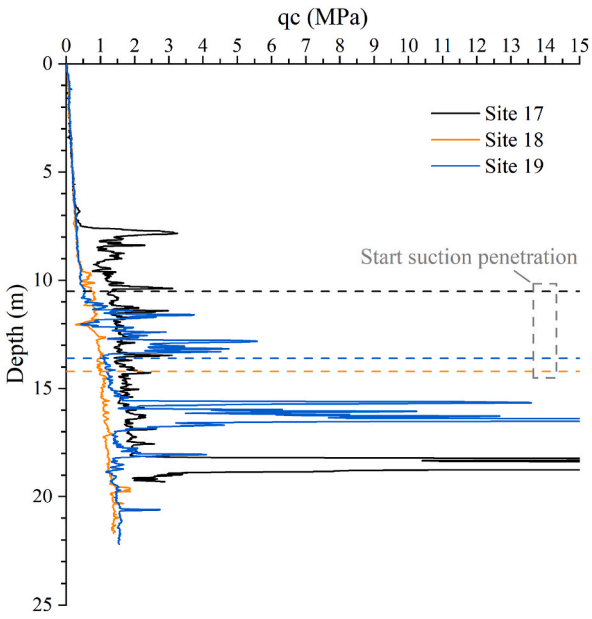

Fig. 13. Cone penetration resistance for (a) Site 17; (b) Site 18; (c) Site 19.

But in practical engineering, TDP is often hardly reached due to the various geotechnical, structural or technical limitations. These challenges, as detailed in Sturm [44], often arise due to various geotechnical, structural, or technical limitations encountered in practical engineering. The section outlines several mitigation measures commonly employed in the field:

Adding the actual weight of the structure by ballast is a direct and useful method, the principle of which is similar to increasing *W* of SBF described in Section 2.1. ***Two way cycles*** of DP is also a alternative approach. Cyclic underpressure and overpressure inside the bucket would cause the vertical reciprocated motion of SBF, which disturbs the soil in the vicinity of the skirts just like the T-bar cyclic tests [45]. The excess pore pressure is generated by the cumulative plastic strain of soil, and then the vertical effective stress is reduced [46]. The penetration resistance is linked to the undrained shear strength in clay, which is related to the vertical effective stress [47]. Hence, a deeper depth of SBF at equal DP is achieved by the cyclic motion as shown in Fig. 14. Besides, changing wall thickness is a preemptive measure where a thicker tip than rest of skirt is set. A gap could be formed inside the skirt where the seepage is facilitated to happen especially suitable for a clay interlayer in sand.

The measurements introduced above make work by means of overcoming the penetration resistance of soil. Another way of ***adding ring stiffeners*** is also a remarkable method. Although the total end area in increased, as well as the tip resistance, the buckling limit is increased accordingly, where the increment of the latter is greater than the former as shown in Fig. 15. These mitigation measures are

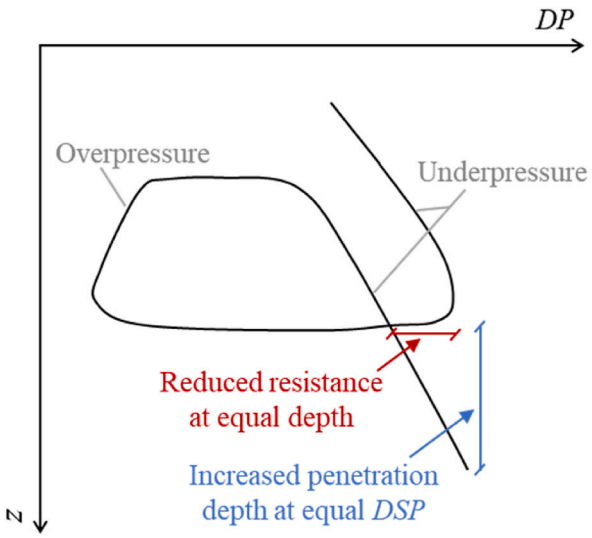

Fig. 14. Schematic diagram of two way cycles to facilitate the SBF penetrating.

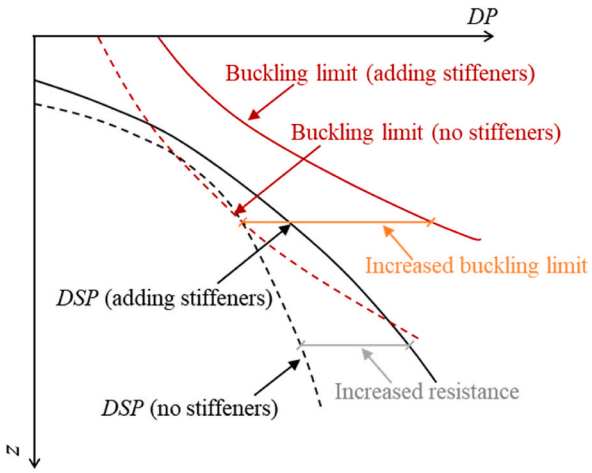

Fig. 15. Schematic diagram of adding stiffeners to facilitate the SBF penetrating.

designed to overcome soil penetration resistance, enhancing the effectiveness of SBF installations in diverse geotechnical contexts. Each approach offers a solution to specific installation challenges, contributing to the successful deployment of SBFs in varying site conditions.

6. Conclusions

This study introduces a new strategy for evaluating design parameters in SBF installations, with a focus on prototype filed cases from the South China Sea. The method begins by classifying the complex and varied soil stratifications into three categories: UDS, PDS, and DS, considering the installation phase and drainage conditions during SBF penetration. Subsequently, both back-calculation and reliability-based estimation methods are employed to derive design parameters for both the self-weight penetration phase and the suction penetration phase. The range of parameters summarised from all cases is suggested and validated for applicability in filed scenarios.

While the study provides a valuable framework, there is room for further improvement. The number of cases analysed, encompassing 16 sites, may not comprehensively represent the diverse geotechnical conditions of the South China Sea in a rigorous sense. However, the proposed strategy for design parameter evaluation is both valid and useful for guiding engineering applications and analysis. Future work is anticipated to expand upon this study, updating or refining the suggested parameters with data from additional SBF installations in other wind farms in China, thereby enhancing the robustness and applicability of the proposed methodology.

CRediT authorship contribution statement

Lunbo Luo: Writing – original draft, Resources, Project administration, Methodology, Investigation, Funding acquisition, Formal analysis, Data curation. **Zhi Li:** Writing – review & editing, Validation, Resources, Project administration, Methodology, Investigation, Funding acquisition, Formal analysis, Data curation. **Zefeng Zhou:** Writing – review & editing, Supervision, Software, Methodology, Investigation, Formal analysis, Data curation, Conceptualization. **Weichen Wang:** Writing – original draft, Visualization, Validation, Software, Methodology, Formal analysis, Data curation, Conceptualization. **Wentao Wang:** Writing – review & editing, Methodology, Formal analysis, Data curation, Conceptualization.

Declaration of competing interest

The authors declare that they have no known competing financial interests or personal relationships that could have appeared to influence the work reported in this paper.

Data availability

Data will be made available on request.

Acknowledgment

The authors acknowledge their research work is supported by the research funding from the China Three Gorges Corporation (No. WWKY-2021-0441, No.202203230).

References

[1] Fu D, Zhang Y, Yan Y, Jostad HP. Effects of tension gap on the holding capacity of suction anchors. Mar Struct 2020;69:102679. https://doi.org/10.1016/j.marstruc.2019.102679.
[2] He B, Jiang J, Cheng J, Zheng J, Wang D. The capacities of tripod bucket foundation under uniaxial and combined loading. Ocean Eng 2020;220:108400. https://doi.org/10.1016/j.oceaneng.2020.108400.
[3] Zhang W, Zhou Z, Pradhan D, Wang P, Jin H. Design considerations of drag anchors in cohesive soil for floating facilities in the South China sea. Mar Struct 2020;81. https://doi.org/10.1016/j.marstruc.2021.103101.
[4] Sheng J, Zhang Y, Xu H, Teng Y, Huang W, Yan H, Ren B, et al. Experience from installation of two suction bucket jacket foundations in layered soils. Mar Georesour Geotechnol 2022. https://doi.org/10.1080/1064119X.2022.2149370.
[5] Houlsby GT, Byrne BW. Suction caisson foundations for offshore wind turbines and anemometer masts. Wind Eng 2000;24(4):249–55.
[6] Andersen KH, Murff JD, Randolph MF, Clukey EC, Erbrich CT, Jostad HP, Hansen B, Aubeny C, Sharma P, Supachawarote C. Suction anchors for deepwater applications. In: Proceedings of the 1st international symposium on frontiers in offshore geotechnics; 2005. p. 3–30. Perth.
[7] Chen W, Randolph MF. External radial stress changes and axial capacity for suction caissons in soft clay. Geotechnique 2007;57(6):499–511.
[8] Ragni R, Bienen B, O'Loughlin CD, Stanier SA, Morgan N. Observations of the effects of a clay layer on suction bucket installation in sand. J Geotech Geoenviron 2020;146:4020020. https://doi.org/10.1061/(ASCE)GT.1943-5606.0002217.
[9] Ibsen LB, Brincker R. Design of a new foundation for offshore wind turbines. Society for Experimental Mechanics 2004:359–66.
[10] Zhou H, Randolph MF. Large deformation analysis of suction caisson installation in clay. Can Geotech J 2006;43(12):1344–57.
[11] Tran MN, Randolph MF, Airey DW. Installation of suction caissons in sand with silt layers. J Geotech Geoenviron Eng 2007;133(10):1183–91.
[12] Ragni R, Bienen B, Stanier S, O'Loughlin C, Cassidy M. Observations during suction bucket installation in sand. Int J Phys Model Geotech 2020;20:132–49. https://doi.org/10.1680/jphmg.18.00071.
[13] Klinkvort RT, Sturm H, Andersen KH. Penetration model for installation of skirted foundations in layered soils. J Geotech Geoenviron 2019;145:4019085. https://doi.org/10.1061/(ASCE)GT.1943-5606.0002106.
[14] Madsen S, Andersen LV, Ibsen LB. Numerical buckling analysis of large suction caissons for wind turbines on deep water. Eng Struct 2013;57:443–52. https://doi.org/10.1016/j.engstruct.2013.09.041.
[15] API. (American Petroleum Institute). Recommended practice for planning, designing, and constructing fixed offshore platforms - working stress design. twenty-first ed. Washington, D.C., USA: API; 2007.
[16] Feld T. Suction Buckets: a new innovation foundation concept, applied to offshore wind turbines. 2001. Aalborg,Denmark (Aalborg Universitetsforlag).
[17] Senders M, Randolph MF. CPT-based method for the installation of suction caissons in sand. J Geotech Geoenviron Eng 2009;135(1):14–25.
[18] Lehane BM, Schneider JA, Xu X. The UWA-05 method for prediction of axial capacity of driven piles in sand. Proceedings of the 1st International Symposium on Frontiers in Offshore Geotechnics 2005:683–9. https://doi.org/10.1201/noe0415390637.ch76.
[19] Xu X, Lehane BM, Schneider JA. Evaluation of end-bearing capacity of open-ended piles driven in sand from CPT data. Proceedings of the 1st International Symposium on Frontiers in Offshore Geotechnics 2005:725–31. https://doi.org/10.1201/noe0415390637.ch82.
[20] Erbrich CT, Tjelta TI. Installation of bucket foundations and suction caissons in sand - geotechnical performance. In: Proc., 31st annual offshore technology conf. Houston: Society of Petroleum Engineers; 1999. p. 725–35. https://doi.org/10.4043/10990-MS.
[21] Bye A, Erbrich C, Rognlien B, Tjelta TI. Geotechnical design of bucket foundations. In: Proc., 27th annual offshore technology conf. Houston: Society of Petroleum Engineers; 1995. p. 869–83. https://doi.org/10.4043/7793-MS.
[22] Lunne T, Powell JJ, Robertson PK. Cone penetration testing in geotechnical practice. New York, USA: CRC Press; 2002.
[23] Aas P.M., Saue M., Aarsnes J. Design predictions and measurements during installation of suction anchors with and without water-flow system to help installation through layered soil profiles. Offshore Technology Conference: OnePetro, OTC-20294-MS,2009.
[24] Bienen B, Klinkvort RT, O'Loughlin CD, Zhu F, Byrne BW. Suction caissons in dense sand, part I: installation, limiting capacity and drainage. Geotechnique 2018;68(11):937–52.
[25] Alexander CR, Demaster DJ, Nittrouer CA. Sediment accumulation in a modern epicontinental-shelf setting: the yellow sea. Mar Geol 1991;98:51–72. https://doi.org/10.1016/0025-3227(91)90035-3.
[26] Wang Y. The mudflat system of China. Can J Fish Aquat Sci 1983;40:160–71. https://doi.org/10.1139/f83-278.
[27] Qiu C, Wang W, Yan Y, Fu D, Yan S. The optimisation of anti-overturning capacities for tripod suction bucket foundations in clay. Ocean Eng 2022;264:112496. https://doi.org/10.1016/j.oceaneng.2022.112496.
[28] Rusaas P, Giske SR, Barrett G, Marine A, Christiansen PE, Baerheim M. Design, operations planning and experience from the marine operations for the europipe jacket with bucket foundations. In: Proc., 27th annual offshore technology conf. Houston: Society of Petroleum Engineers; 1995. p. 885–95. https://doi.org/10.4043/7794-MS.
[29] Tjelta TI. Geotechnical experience from the installation of the europipe jacket with bucket foundations. In: Proceedings of the annual offshore technology conf; 1995. p. 897–908. https://doi.org/10.4043/7795-MS.
[30] Andersen KH, Jostad HP, Dyvik R. Penetration resistance of offshore skirted foundations and anchors in dense sand. J Geotech Geoenviron 2008;134:106–16. https://doi.org/10.1061/(ASCE)1090-0241(2008)134:1(106).
[31] DNV - Norske Veritas Det. Geotechnical design and installation of suction anchors in clay. Hovik, Norway: DNV; 2021.
[32] DNV. Offshore soil mechanics and geotechnical engineering. Offshore standard (DNVGL-RP-C212). Oslo, Norway: DNV; 2021.
[33] OWA. Suction installed caisson foundations for offshore wind: design guidelines. London, United Kingdom: Carbon Trust; 2019.
[34] Cotter O. Installation of suction caisson foundations for offshore renewable energy structures. Oxford: University of; 2010.
[35] Skempton AW. The bearing capacity of clays. Selected papers on soil mechanics. 1951. p. 50–9. https://doi.org/10.1680/sposm.02050.0008.
[36] Vandenboer K, Van Beek VM, Bezuijen A. 3d character of backward erosion piping. Geotechnique 2018;68:86–90. https://doi.org/10.1680/jgeot.16.P.091.
[37] Bakmar CL. Design of offshore wind turbine support structures: selected topics in the field of geotechnical engineering. Aalborg University; 2009.
[38] Lunne T. Analysis of full-scale measurements on gravity platforms. Oslo, Norway: Norwegian Geotechnical Institute; 1982.
[39] Chow S, O'Loughlin C, Zhou Z, White D, Randolph M. Penetrometer testing in a calcareous silt to explore changes in soil strength. Geotechnique 2020;70(12):1160–73.
[40] Finnie I, Randolph M. Punch-through and liquefaction induced failure of shallow foundations on calcareous sediments. In: *Proc.,* seventh international conference on the behaviour of offshore structures *conf*. Massachusetts, USA: Pergamon; 1994. p. 217–30.
[41] Liu K, Wang D, Zheng J. Numerical investigation of spudcan penetration under partially drained conditions. Ocean Eng 2022;244:110425. https://doi.org/10.1016/j.oceaneng.2021.110425.
[42] Liu K, Wang D, Zheng J. Determination of the coefficient of consolidation by piezocone tests under partially drained conditions. Geotechnique 2022. https://doi.org/10.1680/jgeot.22.00064.
[43] Robertson PK. Soil classification using the cone penetration test. Can Geotech J 1990;27:151–8. https://doi.org/10.1139/t90-014.
[44] Sturm H. Design aspects of suction caissons for offshore wind turbine foundations. In: Proc., 19th int. Conf. On soil Mechanics and geotechnical engineering. Seoul, South Korea: Korean Geotechnical Society; 2017. p. 75–93.
[45] Yuan F, White DJ, O'Loughlin CD. The evolutionof seabed stiffness during cyclic movement in a riser touchdown zone on soft clay. Geotechnique 2017;67:127–37. https://doi.org/10.1680/igeot.15.P161.
[46] Zhou Z, White DJ, O'Loughlin CD. An effective stress framework for estimating penetration resistance accounting for changes in soil strength from maintained load, remoulding and reconsolidation. Geotechnique 2018;69:1–46. https://doi.org/10.1680/jgeot.17.p.217.

[47] Zhou Z, O'Loughlin CD, White DJ. An effective stress analysis for predicting the evolution of SCR-seabed stiffness accounting for consolidation. Thomas. Géotechnique 2020;70:448–67. https://doi.org/10.1680/JGEOT.18.P.313.
[48] Ma Z., Liu D., Liu B., Zhang Y., Andersen K. Installation of Suction Bucket Foundations in Layered Soils in Southern China. The 32nd International Ocean and Polar Engineering Conference, Shanghai, China, June 2022, ISOPE-I-22-105.
[49] Hong Z, Zhou Z, Liu W, Yan Y, Fu D, Yan S. Analysis of walking rate for subsea pipelines neighbouring the pipeline end terminations/pipeline end manifolds. Ocean Eng 2020;218:108087. https://doi.org/10.1016/j.oceaneng.2020.108087.